RSC Advances

PAPER

View Article Online
View Journal | View Issue

Cite this: *RSC Adv.*, 2018, **8**, 18663

Silicalite-1 zeolite acidification by zinc modification and its catalytic properties for isobutane conversion†

Guodong Liu,[a] Jiaxu Liu,[a] Ning He,[a] Cuilan Miao,[a] Jilei Wang,[a] Qin Xin[b] and Hongchen Guo*[a]

Received 21st March 2018
Accepted 14th May 2018

DOI: 10.1039/c8ra02467g

rsc.li/rsc-advances

A series of Zn-modified Silicalite-1 (S-1) zeolites (Zn_x/S-1) were prepared by the wetness-impregnation method and applied in the catalytic conversion of isobutane. The structure and location of Zn species in Zn_x/S-1 were investigated using UV-Vis and N_2 physical adsorption. The acidity and origin of the acid sites in Zn_x/S-1 were studied by NH_3-temperature programmed desorption and Fourier-transform infrared analysis. The catalytic performance of Zn_x/S-1 for isobutane conversion was investigated in a fixed-bed microreactor. In the experiments, the acidity of S-1 zeolite was dramatically increased by modification with Zn, with both Lewis and Brønsted sites identified in Zn_x/S-1. The relationship between Brønsted acid sites and Zn–OH groups on ZnO clusters of Zn_x/S-1 was also revealed for the first time. Furthermore, Zn_x/S-1 catalysts exhibited excellent catalytic performances in both isobutane dehydrogenation and butene isomerization reactions. A high selectivity of total butene products ranging from 84.6 to 97.2 was achieved on the catalysts with different Zn loadings. Moreover, the linear correlation between isobutane conversion and the acid amount (determined by NH_3-TPD) confirmed that the weak-to-medium acid sites in Zn_x/S-1 should play a key role in isobutane conversion.

1 Introduction

Silicalite-1 (S-1) zeolite is an aluminum-free crystalline silicate with the same MFI topological framework as the Al-containing ZSM-5 zeolite. Generally, crystalline S-1 zeolites are chemically inert because their interior structure contains only unreactive siloxane (Si–O–Si) bridges.[1] The presence of defective sites in their lattice can facilitate the formation of weak acidic centers (derived from silanol groups), which have been reported as active Beckmann rearrangement catalysts.[2–4] Although the amount of weak acid sites and, to some extent, the acidic strength of S-1 zeolite can be modulated by changing the crystallization conditions or through post-synthesis treatment,[2,5,6] its catalytic properties remain limited. In contrast, ZSM-5 is a strongly acidic zeolite that can catalyze several reactions, including olefin oligomerization, aromatic alkylation, toluene disproportionation, methanol-to-hydrocarbon conversions (including MTG, MTO, MTP), and light hydrocarbon cracking and aromatization.[7–11] This clearly indicates that the acidity of S-1 zeolite needs to be increased to broaden its catalytic applications.

The conversion of light alkanes, such as propane and isobutane, into their corresponding value-added alkenes has received much attention. Currently, Pt/Al_2O_3 and Cr_xO_3/Al_2O_3 catalysts are employed industrially to produce propylene and isobutene from the non-oxidative dehydrogenation of propane and isobutane, respectively.[12] However, these catalysts have drawbacks because Pt is expensive and has limited availability, while Cr_xO_3/Al_2O_3 is not environmentally friendly owing to its toxicity.[13] Therefore, the development of novel catalysts with superior catalytic efficiency for light alkane non-oxidative dehydrogenation is highly desirable. It has been accepted that Zn-containing catalysts were active in the dehydrogenation of alkanes.[14–16,19–21] Zn-modified HZSM-5 zeolites (Zn/ZSM-5) have been reported to be effective catalysts for low-temperature activation of light alkanes, with the modified Zn species playing a key role in light alkane dehydrogenation.[14–16] However, their commercial use in such processes is impeded by their poor alkene selectivity with respect to the formation of large amounts of cracked dry gas byproducts (C_1 and C_2 hydrocarbons), resulting from the strong acidic character of HZSM-5 zeolite.[17,18] Moreover, zinc titanate catalysts in the form of hydrogels or mixed oxides have also been mentioned in the dehydrogenation of light alkanes.[19,20] Zinc titanate is an environmentally friendly material and of low cost. However, the overall activity of the

[a]*Department of Catalytic Chemistry and Engineering, State Key Laboratory of Fine Chemicals, Dalian University of Technology, Dalian 116012, P. R. China. E-mail: hongchenguo@dlut.edu.cn*

[b]*State Key Laboratory of Catalysis, Dalian Institute of Chemical Physics, Chinese Academy of Sciences, Dalian 116023, P. R. China*

† Electronic supplementary information (ESI) available: XRF, SEM and TEM images, N_2 adsorption and desorption isotherms, the relative crystallinity of catalysts, XRD patterns, the acid amount of catalysts. See DOI: 10.1039/c8ra02467g

catalyst was found to be limited or the selectivity declined rapidly as a function of reaction time. Recently, isolated Zn^{2+} species deposited on a silica support were found to be active in propane dehydrogenation.[21] The high propylene selectivity was attributed to the absence of Brønsted acid sites on the Zn/SiO_2 catalyst. However, the catalyst is not so stable enough that its activity only remained half of the initial activity in 12 h.

The activation of propane over Zn-modified S-1 zeolite (denoted as Zn/S-1) has been studied by employing *in situ* ^{13}C MAS NMR and IR spectroscopic techniques in 2006.[15] It was proposed that propane was activated through dissociative adsorption over zinc oxide species, followed by propene evolution and recombinative desorption of dihydrogen. On the other hand, the acidity of Zn-modified HZSM-5 zeolite (Zn/HZSM-5) was reported to play a key role in the transformation of light alkanes. However, few study related to the effect of acid sites of Zn/S-1 on alkane dehydrogenation was reported, probably because the acidity of S-1 zeolite is negligible compared with that of HZSM-5 zeolite. Moreover, the influence of Zn modification on the acidity of S-1 zeolite and the role of these acid sites in light alkane conversion is yet unclear. Therefore, a series of Zn-modified S-1 catalysts was prepared in this work. The acidity and origin of acidity of these Zn/S-1 catalysts were characterized by NH_3-temperature programmed desorption (TPD) and Fourier-transform infrared (FT-IR) spectroscopy analysis. Furthermore, the catalytic properties of these Zn/S-1 catalysts in isobutane conversion were investigated using a fixed-bed microreactor.

2 Experimental

2.1 Catalyst preparation

S-1 zeolite was synthesized according to a reported procedure for the synthesis of TS-1,[22] except that no titanium source was used. Typically, tetraethyl orthosilicate (TEOS; Sinopharm Chemical Reagent Co., Ltd), tetrapropylammonium hydroxide (TPAOH; 25 wt% aqueous solution, Sinopharm), and distilled deionized water were mixed to form a clear solution with a SiO_2/TPAOH/H_2O ratio of 1 : 0.3 : 30. The solution was hydrolyzed at 60 °C in a water bath for 3 h with magnetic stirring to give a homogeneous sol that was then transferred to a Teflon-lined autoclave and crystallized at 170 °C for 24 h. The as-synthesized precipitate was collected by filtration, washed several times with deionized water, and dried at 110 °C overnight. The zeolite products were then calcined at 550 °C for 6 h for further characterization or use.

Zn-modified zeolite catalysts were prepared using a wetness-impregnation method. The calcined S-1 zeolite was impregnated with an aqueous solution of $Zn(NO_3)_2 \cdot 6H_2O$ (Sinopharm Chemical Reagent Co., Ltd) in a water bath at 80 °C for 3 h. The impregnated zeolite was then dried at 110 °C for 12 h and calcined at 550 °C for 6 h to obtain the Zn/S-1 samples. The desired Zn loadings were achieved by adjusting aqueous solution of $Zn(NO_3)_2 \cdot 6H_2O$ with the appropriate concentration. The modified S-1 zeolites with different Zn loadings were denoted as Zn_x/S-1, where x is the Zn loading amount in wt%. For comparative catalytic tests in isobutane conversion, a 6.0 wt% Zn-modified HZSM-5 zeolite (crystal size, 100–200 nm; SiO_2/Al_2O_3 molar ratio, 26 : 1) was also prepared using the same impregnation method (denoted as $Zn_{6.0}$/ZSM-5).

2.2 Catalyst characterization

Powder X-ray diffraction (XRD) patterns were collected on a Rigaku D/max-2004 diffractometer with a Cu Kα radiation source (40 kV, 100 mA). Measurements were conducted in the 2θ range of 5–80° with a scanning speed of 2° min^{-1}. X-Ray Fluorescence spectrometry (XRF) was conducted on a Bruker SRS 3400 instrument. Field emission scanning electron microscopy (FE-SEM) images of crystal morphologies were obtained using a Hitachi S-4800 microscope. The distribution of Zn species on the modified catalysts was examined by UV-Vis spectrophotometry, conducted on a JASCO V-550 spectrometer with $BaSO_4$ as the reference. High resolution transmission electron microscopy (HRTEM) measurements were taken on a JEM-2100F electron microscope with an acceleration voltage of 200 kV.

N_2 physical adsorption–desorption isotherms were measured on a Micromeritics ASAP 2020 instrument at −196 °C to determine the textural properties. Prior to measurement, the samples (sieve fraction, 380–830 μm) were degassed under vacuum at 350 °C for 6 h. The specific surface area was calculated by the Brunauer–Emmett–Teller (BET) method using the adsorption branch in the P/P_0 range 0.10–0.15. The pore volumes were estimated at the P/P_0 point of 0.99. The microporosity and mesoporosity of the samples was discriminated using the *t*-plot method.

NH_3-TPD was performed on a Quantachrome ChemBet 3000 chemisorb instrument to investigate the total acidity of the catalysts. Sample pellets (150 mg; sieve fraction, 380–830 μm) were pretreated under helium (He) at 600 °C for 1 h. After cooling to 100 °C, a mixed gas of 5% NH_3 in He was passed through the catalyst bed to allow ammonia adsorption for 30 min. The cell was then purged with He flow (50 mL min^{-1}) for 30 min to remove all NH_3 not chemically adsorbed. The NH_3-TPD profiles were recorded by heating the cell to 600 °C at a ramping rate of 16 °C min^{-1}.

FT-IR of adsorbed NH_3 (FT-IR-NH_3) was used to determine the Lewis and Brønsted acidities of the catalysts. FT-IR-NH_3 spectra were collected on a Nicolet 6700 FT-IR spectrometer (4 cm^{-1} optical resolution with one level of zero-filling for the Fourier transform). First, about 15 mg of sample was pressed into a self-supporting wafer (diameter, 13 mm) and then treated in a cuvette *in situ* under vacuum (10^{-3} Pa) at 400 °C for 4 h. NH_3 adsorption was conducted with admittance of an ammonia flow of 30 mL min^{-1} into the cuvette for 30 min at ambient temperature. The wafer was then subjected to vacuum treatment at 150, 300, and 450 °C for 30 min each. Finally, the measured spectra were collected.

To determine the catalyst acidity of the surface hydroxyl groups, FT-IR spectra of surface hydroxyl groups with ammonia absorption (OH-FT-IR-NH_3) were recorded using a Nicolet iS10 FT-IR spectrometer. The samples were pressed into self-supporting thin wafers (approximately 15 mg) and

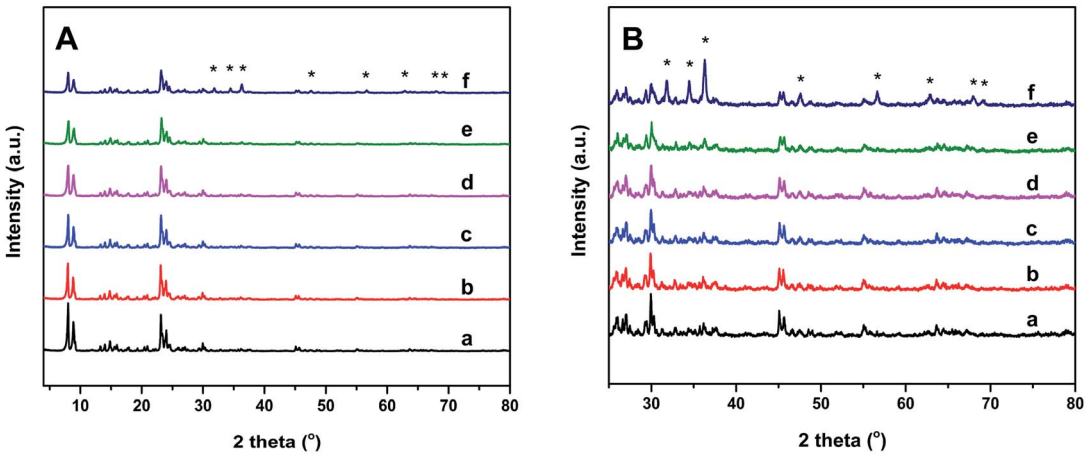

Fig. 1 XRD patterns (A) and the magnified patterns (B) of S-1 (a), $Zn_{1.0}$/S-1 (b), $Zn_{3.0}$/S-1 (c), $Zn_{6.0}$/S-1 (d), $Zn_{8.0}$/S-1 (e) and $Zn_{12.0}$/S-1 (f). (The asterisk labels show the diffraction peaks of ZnO crystal with wurtzite structure).

decontaminated at 400 °C under vacuum (10^{-3} Pa) for 4 h in a quartz IR cell equipped with CaF_2 windows. An ammonia gas stream (30 mL min^{-1}) was passed through the sample cell at 150 °C for 30 min to allow ammonia adsorption. Evacuation treatment (10^{-3} Pa) was conducted for 30 min at the same temperature. After cooling to room temperature, OH-FT-IR-NH_3 spectra were recorded by subtracting the blank background spectrum (recorded using an empty IR cell without sample). Spectra were recorded in the range 4000–400 cm^{-1} with a resolution of 4 cm^{-1}.

2.3 Catalytic tests

Isobutane conversion tests were performed in a fixed-bed microreactor (i.d., 6 mm) under atmospheric pressure. The catalyst loading for each run was about 200 mg. Prior to activity tests, catalysts (d_p = 20–40 mesh) were activated *in situ* at 550 °C for 1 h under nitrogen flow, and then prereduced under 5% H_2 in N_2 gas flow (50 mL min^{-1}, standard temperature and pressure) at 500 °C for 30 min. The isobutane feedstock was diluted with nitrogen (employed as a calibrating gas) to give a 50 : 50 (v/v) mixture. The flow rates of isobutane and nitrogen were controlled separately using mass flow meters. For catalytic activity tests, the mixing gas was fed at a gas hourly space velocity (GHSV) of about 1200 h^{-1}, with the reaction conducted at 550 °C and atmospheric pressure. Effluent hydrocarbon products were analyzed using on-line gas chromatography (GC; Shimadzu GC-14B, OV-1 capillary column 50 m × 0.20 mm, flame ionization detector).

The isobutane conversion ($C_{isobutane}$) and product selectivity (S_i) were calculated using the following equations:

$$C_{isobutane} = (\sum A_i - A_{isobutane})/\sum A_i \times 100\% \quad (1)$$

$$S_i = A_i/(\sum A_i - A_{isobutane}) \times 100\% \quad (2)$$

where A_i and $A_{isobutane}$ are the corrected chromatographic areas of a specific compound and residual isobutane, respectively.

3 Results and discussion

3.1 Catalyst characterization

SEM, XRD, and N_2 physical adsorption–desorption isotherms were measured to assess the effect of the Zn dopant on the structures of the Zn_x/S-1 catalysts. The SEM images (see Fig. S1†) showed that the mean size of parent S-1 zeolite was around 100 nm. The introduction of Zn species by impregnation has little influence on the crystal size and the morphology of parent S-1 zeolite. Structural changes in Zn_x/S-1 catalysts were also analyzed using XRD patterns. As shown in Fig. 1, five characteristic diffraction peaks of MFI structure were found at 2θ = 7.9, 8.8, 23.1, 23.8 and 24.3 in all catalysts. No diffraction signal for Zn species was observed at Zn content below 8.0 wt%, indicating that Zn species were highly dispersed. Nevertheless, characteristic peaks of the ZnO phase with a wurtzite structure[23] (denoted with asterisks in Fig. 1A and B) were presented in $Zn_{12.0}$/S-1. When the amount of Zn added was too high, Zn species seemed not to be uniformly dispersed in the zeolite channels, but formed large wurtzite-structured ZnO particles on the zeolite surface. The average particle size of ZnO particles was estimated to be 4.8 nm by using the Scherrer's equation. Fig. S2† shows the HRTEM images of $Zn_{6.0}$/S-1 and $Zn_{12.0}$/S-1 catalysts. There are a number of ZnO particles reside on the external surface of $Zn_{12.0}$/S-1 catalyst, while no clear pattern of ZnO particles has been observed on the outside surface of $Zn_{6.0}$/S-1. Moreover, in comparison with parent S-1 zeolite, the relative crystallinity of Zn_x/S-1 catalysts gradually decreased (see Table S2†), which was probably attributed to the high X-ray absorption coefficient of impregnated metal species.[24,25] The textural properties of Zn_x/S-1 catalysts were determined from N_2 physical adsorption–desorption, as summarized in Table 1. At low Zn loadings (1.0 wt% and 3.0 wt%), the specific surface area of Zn_x/S-1 decreased slightly with increasing Zn loading. This indicated that subnanometric ZnO clusters inside the zeolitic pores or channels only had a small effect on the textural properties of the S-1 zeolite. However, at high Zn loadings (above

Table 1 N_2 adsorption–desorption data of Zn_x/S-1 catalysts

Zn loading (wt%)	S_{BET} ($m^2\ g^{-1}$)	S_{Micro} ($m^2\ g^{-1}$)	S_{extern} ($m^2\ g^{-1}$)	V_{pores} ($cm^3\ g^{-1}$)	V_{micro} ($cm^3\ g^{-1}$)	V_{meso} ($cm^3\ g^{-1}$)
0.0	390	239	150	0.27	0.11	0.16
1.0	383	239	143	0.27	0.11	0.16
3.0	370	228	141	0.26	0.10	0.15
6.0	325	245	80	0.20	0.10	0.10
8.0	290	217	72	0.20	0.10	0.10
12.0	269	195	73	0.21	0.09	0.12

6.0 wt%), the specific surface area of Zn_x/S-1 declined rapidly with increasing Zn loading, mainly due to decreases in external surface area (from 150 $m^2\ g^{-1}$ to 72 $m^2\ g^{-1}$) and mesoporosity (from 0.16 $m^3\ g^{-1}$ to 0.10 $m^3\ g^{-1}$). Furthermore, the microstructure characteristics were slightly disrupted. These data showed that large ZnO particles were mainly deposited on the external surface and blocked mesopore openings in S-1 zeolite.

UV-Vis spectra of Zn_x/S-1 catalyst are shown in Fig. 2. Generally, the modification of S-1 with Zn leads to the appearance of two new bands at about 265 and 365 nm, corresponding to subnanometric ZnO clusters inside zeolitic pores and large ZnO crystals on the external zeolite surface, respectively.[15,23] For $Zn_{1.0}$/S-1 and $Zn_{3.0}$/S-1 samples, the band at 265 nm was significant, while the band at 365 nm was almost nonexistent, suggesting that the two catalysts mainly comprised subnanometric ZnO clusters. In contrast, both bands were present in samples with Zn loadings above 6.0 wt%. Increasing Zn loading in these catalysts enhanced both bands, with the intensity of the band at 365 nm increasing much faster. These observations showed that the Zn_x/S-1 samples with higher Zn loadings (x = 6.0–12.0) contained not only ZnO clusters inside S-1 zeolitic pores, but also large ZnO crystals located on the external surface. The increased Zn loading mainly facilitated the formation of large ZnO crystals.

3.2 Acidity enhancement by Zn modification

The acid amount and strength of S-1 and Zn-modified sample $Zn_{6.0}$/S-1 were investigated using NH_3-TPD. For comparison, the acidities of HZSM-5 (SiO_2/Al_2O_3 molar ratio, 26 : 1) and $Zn_{6.0}$/HZSM-5 were also tested. As shown in Fig. 3A, the whole NH_3 desorption profile for the parent S-1 zeolite was approximately a straight line. Almost no NH_3 molecules were adsorbed on S-1, demonstrating its weak acidic character compared with that of HZSM-5. Notably, the NH_3 desorption peak of the $Zn_{6.0}$/S-1 sample was quite strong, although the acid amount remained much lower than that of HZSM-5 and $Zn_{6.0}$/HZSM-5. This clearly showed that impregnation with Zn significantly enhanced the acidity of the S-1 zeolite. We also compared the NH_3-TPD profiles of the Zn_x/S-1 catalysts, which exhibited two distinct desorption peaks at 267 and 375 °C (see Fig. 3B), corresponding to weak and medium acidic sites, respectively. Furthermore, it was also feasible to gradually increase the amount of acid sites in the S-1 zeolite by increasing the loading of Zn until the maximum value was reached, as shown in Fig. 4. Detailed information on the calculated statistical results of acid amount is shown in Table S3.† For the parent S-1 used herein, the maximum Zn loading was around 6.0–8.0 wt%. When the Zn loading was low (below 3.0%), the increase in Zn loading dramatically increased the acidity of the S-1 zeolite. However, when the Zn loading was high (in the range 3.0–8.0 wt%), the overall acid amount in the modified S-1 zeolite reached its maximum value, with the increasing trend with Zn loading becoming marginal.

The acidity of Zn_x/S-1 zeolites was further studied using ammonia-adsorbed FT-IR spectra. As shown in Fig. 5A, the strong absorption peak at 1620 cm^{-1} was attributed to asymmetric deformation of ammonia coordinated to Lewis acid sites, which usually appears in the bending vibration region of 1700–1300 cm^{-1} and indicates that Zn modification resulted in the formation of an appreciable amount of Lewis acid sites in Zn_x/S-1.[26–29] The variation trend in the intensity of this peak was in agreement with the change in the NH_3-TPD results. However, the existence of Brønsted acid sites in Zn_x/S-1 required further confirmation because the IR bands corresponding to ammonium ion deformation vibrations were obscure. In contrast, as shown in Fig. 5A and the magnified range of 3500–3000 cm^{-1} in Fig. 5B, in addition to the apparent bands in the range 3350–3200 cm^{-1}, which were attributed to ammonia coordination on Lewis acid sites, two weak yet clear absorption peaks at 3220 and 3190 cm^{-1} emerged in the N–H stretching region.[26,28] It was clear that Zn modification not only produced a number of Lewis

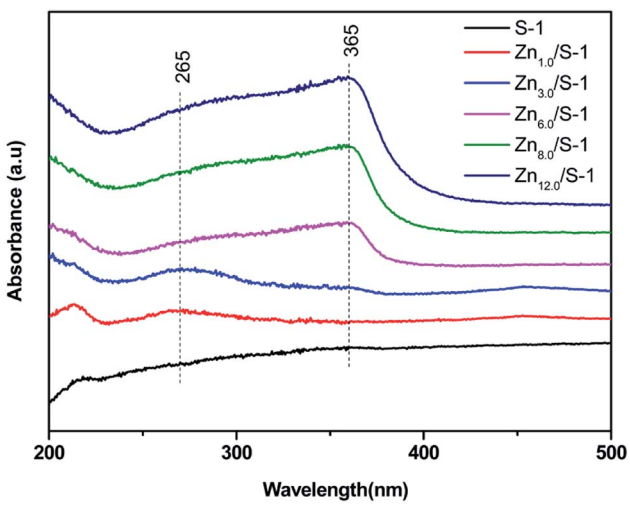

Fig. 2 UV-Vis spectra of Zn_x/S-1 (x from 0.0 to 12.0).

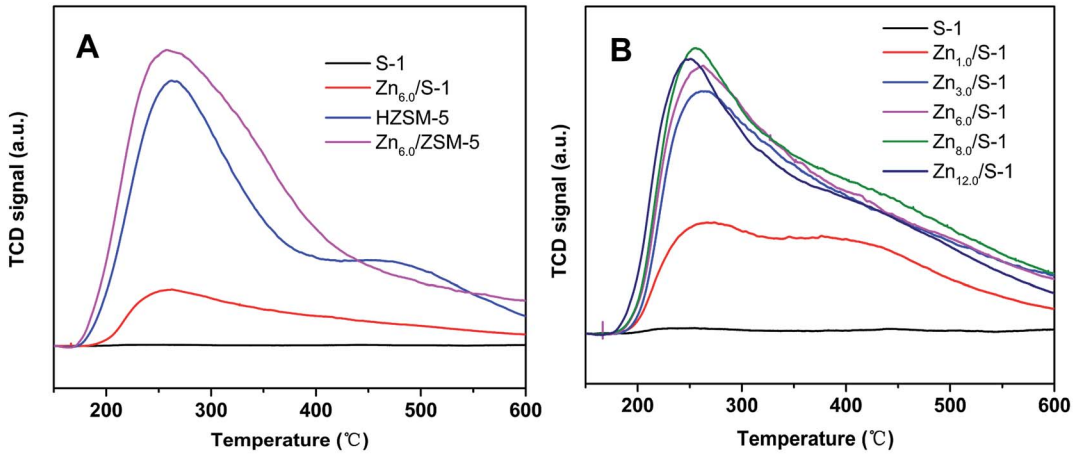

Fig. 3 NH_3-TPD profiles of (A) S-1, $Zn_{6.0}$/S-1, HZSM-5 and $Zn_{6.0}$/HZSM-5, and (B) the series Zn_x/S-1 (x from 0.0 to 12.0) samples.

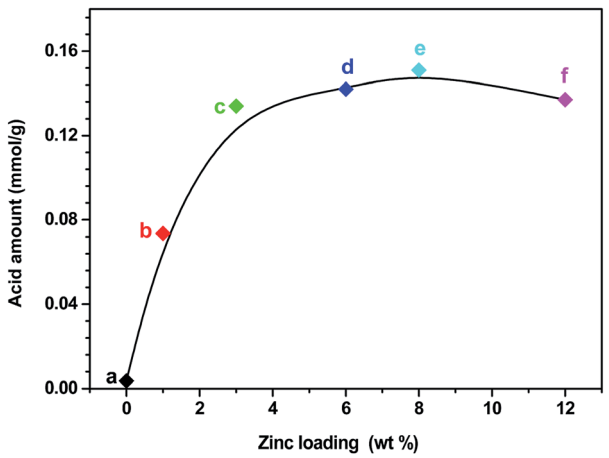

Fig. 4 The relevance of Zn loading and acid amount of S-1 (a), $Zn_{1.0}$/S-1 (b), $Zn_{3.0}$/S-1 (c), $Zn_{6.0}$/S-1 (d), $Zn_{8.0}$/S-1 (e) and $Zn_{12.0}$/S-1 (f), respectively.

acid sites, but also raised some Brønsted acid sites in Zn_x/S-1 catalysts, as disclosed by the two N–H stretching signals. Furthermore, we further detected variations in the spectra with heating and evacuation procedures, as shown in Fig. 6. The bands at 3290, 3220, and 3190 cm^{-1} almost disappeared after evacuation at 450 °C for 30 min, suggesting the acid sites of Zn_x/S-1 were mostly weak to medium. This was in good agreement with the NH_3-TPD results.

3.3 Origin of Zn_x/S-1 acidity

3.3.1 Lewis acid sites in Zn_x/S-1. It is generally accepted that Zn species[14–16,30,31] can provide Lewis acid sites in Zn-modified ZSM-5 or beta zeolite. Similarly, we speculated that the Lewis acid sites in Zn_x/S-1 were also associated with their Zn species. UV-Vis spectra and FT-IR spectroscopy of adsorbed CO results showed that Zn/S-1 contained two Zn species: small ZnO clusters inside the pore and large ZnO crystals on the external surface.[15] Therefore, the Lewis acid sites of Zn_x/S-1 should be provided by ZnO clusters or large ZnO crystals. The UV-Vis

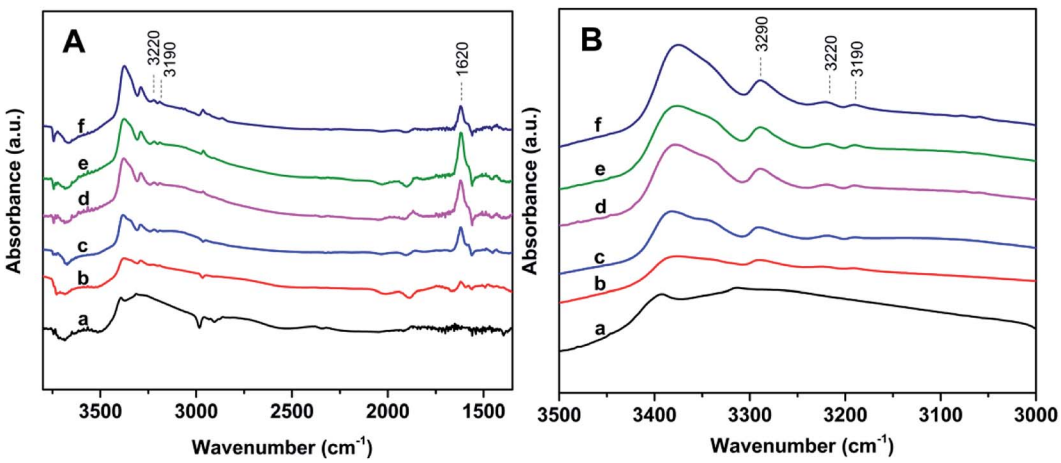

Fig. 5 Ammonia-adsorbed FT-IR spectra (A) and the magnified spectra in the NH-stretching region (B) of the series $Zn_{6.0}$/S-1 Zn_x/S-1 samples: (a) S-1, (b) $Zn_{1.0}$/S-1, (c) $Zn_{3.0}$/S-1, (d) $Zn_{6.0}$/S-1, (e) $Zn_{8.0}$/S-1 and (f) $Zn_{12.0}$/S-1.

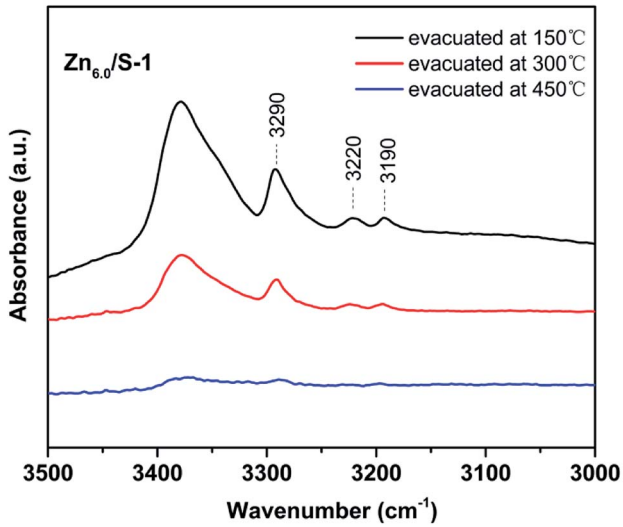

Fig. 6 Ammonia-adsorbed FT-IR spectra of $Zn_{6.0}$/S-1 in the NH-stretching region after evacuation at 150, 300 and 450 °C for 30 min.

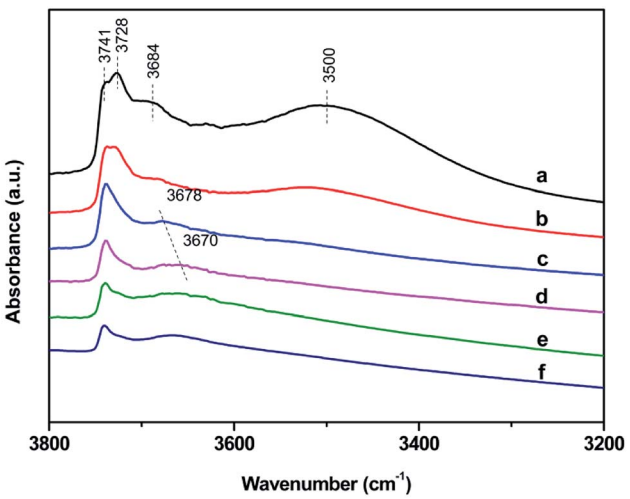

Fig. 7 Infrared hydroxyl stretching region of S-1 (a), $Zn_{1.0}$/S-1 (b), $Zn_{3.0}$/S-1 (c), $Zn_{6.0}$/S-1 (d), $Zn_{8.0}$/S-1 (e) and $Zn_{12.0}$/S-1 (f). Catalysts have been dehydrated at 400 °C for 4 h.

spectra (Fig. 2) showed that subnanometer ZnO clusters inside zeolite pores were the primary Zn species in Zn_x/S-1 at low Zn loadings. In addition to ZnO clusters, most large ZnO crystals were generated on the external surface when the Zn loadings were much higher. In contrast, as shown in Fig. 5A, the ammonia-adsorbed FT-IR spectra clearly indicated a similar change in the quantity of Lewis acid sites of Zn_x/S-1 with the change in peak intensity at 1618 cm^{-1}. The Lewis acid amount in Zn_x/S-1 increased dramatically with increasing Zn loading at low loadings (below 3.0 wt%). This increasing trend slowed as the Zn loading was increased from 3.0 wt% to 8.0 wt%, and then began to decrease when the Zn loading reached 12.0 wt%. From both UV-Vis and ammonia-adsorbed FT-IR spectra, it was easy to conclude that subnanometer ZnO clusters inside S-1 zeolite pores were the major contributors of Lewis acid sites in Zn_x/S-1 catalysts.

3.3.2 Brønsted acid sites in Zn_x/S-1. As shown in the hydroxyl stretching vibration region of the FT-IR spectra (Fig. 7), S-1 zeolite contained isolated silanol groups exposed on the external surface (3741 cm^{-1}), terminal silanol groups located in the internal cavities (3728 cm^{-1}), abundant H-bonded silanols in internal defects as linear chains and/or rings of hydroxylated species (3500 cm^{-1}), and vicinal silanols inside internal pores (3684 cm^{-1}).[1,2] The appearance of these silanol groups indicated the presence of a large number of defect sites in S-1 zeolite. When S-1 zeolite was modified with Zn, these internal silanol groups (bands at 3728, 3684, and 3500 cm^{-1}) and some of the isolated silanol groups (3741 cm^{-1}) exposed at the external surface of S-1 zeolite were found to be dramatically diminished, suggesting that some Zn species in Zn_x/S-1 strongly interacted with the defect sites. Furthermore, a new band at 3678 cm^{-1} was observed in $Zn_{3.0}$/S-1, and redshifted to 3670 cm^{-1} when the Zn loading was increased from 6.0 to 12.0, which was likely due to the formation of external Zn–OH groups on the ZnO clusters.[15]

FT-IR spectra of surface hydroxyl groups with ammonia absorption were also measured to probe the Brønsted acid sites of Zn_x/S-1. To avoid disturbance from hydrogen-bonded species formed by the interaction of NH_3 and intrinsic hydroxyl groups in S-1 zeolite, as shown in Scheme 1,[1] the ammonia-adsorbed catalysts were evacuated at 150 °C for 30 min. After Zn modification, both Lewis and Brønsted acid sites were found in Zn_x/S-1 ($x = 1.0$–6.0), as shown in the (NH) stretching region in Fig. 8B. This result was consistent with the ammonia-adsorbed FT-IR spectra (Fig. 5). In contrast, it was interpreted from Fig. 8A that the residual signals (ν= 3741, 3728, and 3500 cm^{-1}) of silicon hydroxyl groups in Zn_x/S-1 would hardly be disturbed after NH_3 adsorption, indicating that they had no effect on the acidity of Zn_x/S-1. Notably, the bands at 3678 and 3670 cm^{-1}, corresponding to Zn–OH groups on ZnO clusters, were significantly consumed after NH_3 adsorption. The consumption of these silanol group bands at 3678 and 3670 cm^{-1} clearly demonstrated that the Zn–OH groups were associated with

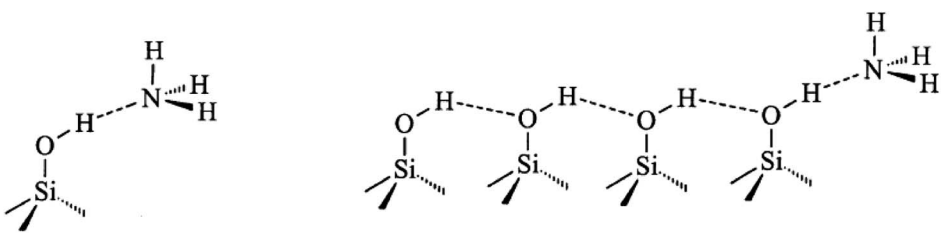

Scheme 1

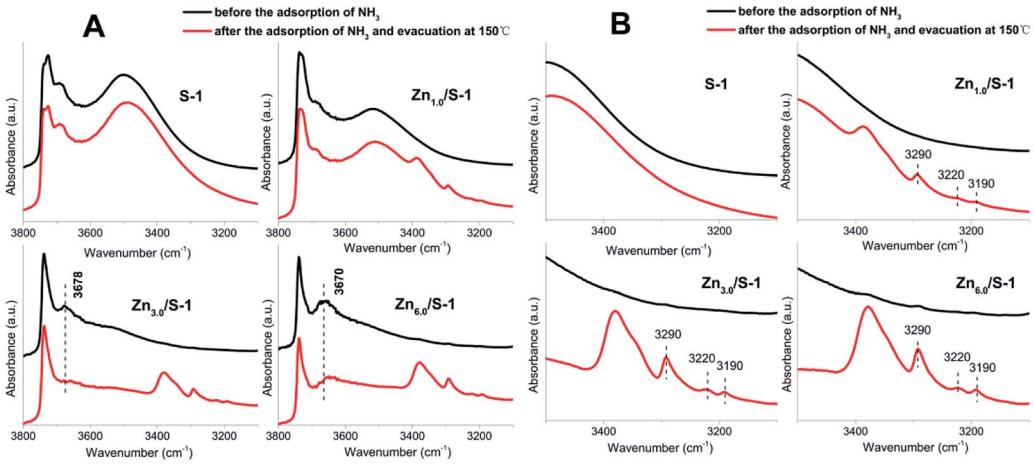

Fig. 8 (A) IR spectra in the ν(OH) and ν(NH) stretching region of Zn_x/S-1 (x from 0.0 to 6.0) before and after the adsorption of NH_3, respectively; (B) corresponding magnified IR spectra in the ν(NH) stretching region.

Brønsted acid sites of Zn_x/S-1. To our knowledge, this relationship between Brønsted acid sites and Zn–OH groups on ZnO clusters of Zn/S-1 is reported here for the first time.

3.4 Catalytic performance

The catalytic conversion of isobutane was tested in a microscale fixed-bed reactor and the results are shown in Table 2. As an effective strategy, Zn modification significantly enhanced the catalytic activity of S-1 zeolite. At 550 °C and atmospheric pressure, the parent S-1 zeolite was completely inactive for isobutane transformation. However, under the same reaction conditions, Zn_x/S-1 catalysts exhibited promoted isobutane conversion rates. In particular, the $Zn_{1.0}$/S-1 and $Zn_{3.0}$/S-1 catalysts led to 27.5% and 60.2% isobutane conversion, respectively. As the Zn content was increased (from 3.0 to 8.0 wt%), the isobutane conversion continued increasing, reaching a maximum isobutane conversion of 66.7%. However, a slight downward tendency in isobutane conversion was observed when the Zn loading reached 12.0 wt%. Despite this, the $Zn_{12.0}$/S-1 catalyst still afforded a good isobutane conversion of 65.5%. Moreover, according to the literature,[32] the iso-butane activity of Zn_x/S-1 (27.5–66.7%) obtained under our experimental conditions is close to that of the commercial Cr_2O_3/Al_2O_3 catalyst (48–65%).

Among the products of isobutane transformation over Zn_x/S-1 catalysts, isobutene was the primary component (about 60%), indicating that Zn modification imparted the catalysts impressive dehydrogenation functions. Furthermore, the presence of substantial amounts of 1-butene and *cis*/*trans*-2-butene among the products indicated that the Brønsted acid sites provided by the Zn–OH groups in S-1 zeolite also played an important role in isobutene isomerization. A high selectivity of isobutene and its isomers ranging from 84.6 to 97.2 was achieved on the catalyst with different Zn loading. Moreover, a small amounts of aromatic products (less than 8%), due to aromatization over the Zn species, and cracked lower hydrocarbon products (C_1–C_3, much less than 8%) were formed because the Brønsted acid strength of Zn_x/S-1 was still relatively weak. In comparison, when isobutane transformation was conducted over the $Zn_{6.0}$/HZSM-5 catalyst, the isobutane conversion rated was nearly 100%, with aromatics obtained as the major product (more than 50%). This reaction also produced a large amount of undesired cracking components (over 40%), which comprised dry gas (C_1 + C_2) and propane in a 2 : 1 ratio. In contrast, the

Table 2 The catalytic performance of iso-butane transformations over S-1, Zn_x/S-1 and $Zn_{6.0}$/ZSM-5 catalysts[a]

		Selectivity (%)					
		Cracking		Dehydrogenation		Aromatization	
Catalyst	Conv. (%)	C_1 + C_2	C_3	$iC_4^=$	$nC_4^=$ + *cis*$C_4^=$ + *trans*$C_4^=$	Total $C_4^=$	Aromatic products
S-1	—	—	—	—	—	—	—
$Zn_{1.0}$/S-1	27.5	0.6	1.6	83.8	13.4	97.2	1.0
$Zn_{3.0}$/S-1	60.2	1.4	2.7	68.2	22.8	91.0	5.0
$Zn_{6.0}$/S-1	61.3	2.1	4.0	64.8	22.9	87.7	6.2
$Zn_{8.0}$/S-1	66.7	2.7	5.1	59.8	24.8	84.6	7.6
$Zn_{12.0}$/S-1	65.5	2.7	5.1	61.7	23.6	85.4	6.8
$Zn_{6.0}$/HZSM-5	99.8	27.3	13.7	0.4	1.3	1.6	57.3

[a] Catalyst loading 200 mg, reactions temperature 550 °C, GHSV 1200 h^{-1}, iso-butane feedstock compositions: iso-butane : N_2 = 50 : 50 (v/v), the results were obtained after 1 h of testing.

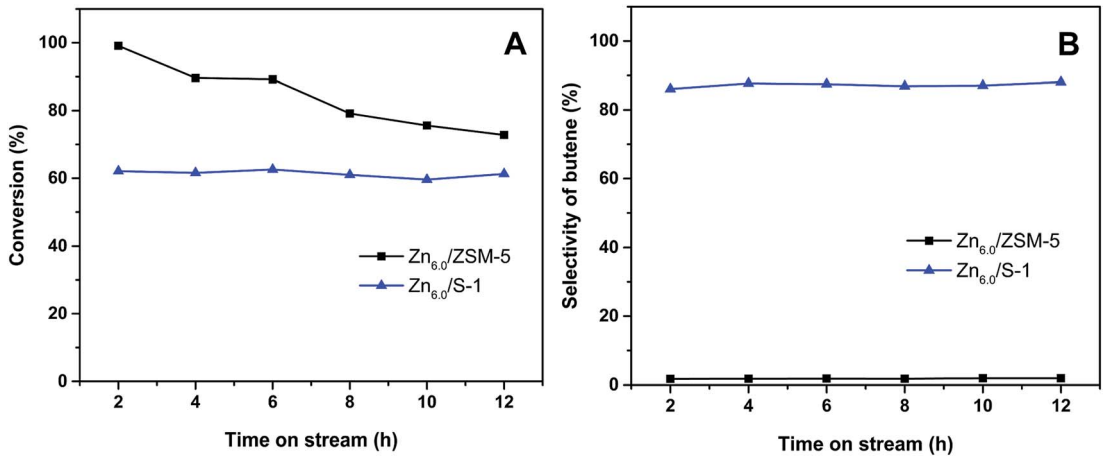

Fig. 9 (A) Conversion of iso-butane and (B) selectivity of butene as a function of reaction time over $Zn_{6.0}$/ZSM-5 and $Zn_{6.0}$/S-1 catalysts.

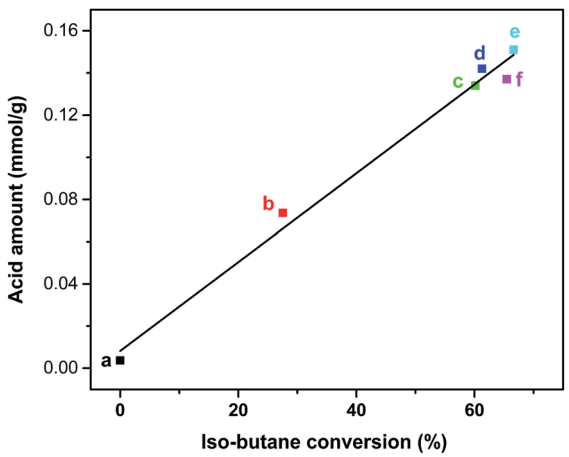

Fig. 10 The relevance between iso-butane conversion and the acid amount of S-1 (a), $Zn_{1.0}$/S-1 (b), $Zn_{3.0}$/S-1 (c), $Zn_{6.0}$/S-1 (d), $Zn_{8.0}$/S-1 (e) and $Zn_{12.0}$/S-1 (f), respectively. (The acid amounts of catalysts were determined by NH_3-TPD).

sum of dry gas and propane byproducts was efficiently suppressed over appropriately modified Zn_x/S-1 catalysts.

The stability of Zn/S-1 catalyst in the conversion of iso-butane was further investigated. As shown in Fig. 9A, slight deactivation was observed over $Zn_{6.0}$/S-1 catalyst during the lifespan of 12 h. However, for $Zn_{6.0}$/HZSM-5 catalyst, the conversion decreased from 99.1% to 72.8% after 12 h. On the other hand, the selectivity of total butene was well-preserved over $Zn_{6.0}$/S-1 catalyst during the 12 h examination (Fig. 9B). These results indicated that Zn_x/S-1 catalysts obtain extraordinary stability in the iso-butane dehydrogenation system. Furthermore, as previously reported,[19–21] zinc titanate and Zn/SiO_2 catalysts also had been considered as the candidates for light alkanes dehydrogenation. However, the zinc titanate catalyst deactivated rapidly when both the selectivity and conversion were kept at a higher level.[19,20] Zn/SiO_2 catalyst exhibited high propylene selectivity in the dehydrogenation of propane.[21] However, the stability is also a big challenge for the industrial applications of Zn/SiO_2 catalyst since the activity can only maintain nearly 50% of the initial value during 12 h test. Therefore, Zn_x/S-1 catalysts exhibited both higher activity and excellent stability in comparison with zinc titanate and Zn/SiO_2 catalysts in the dehydrogenation of alkanes.

By correlating the isobutane conversion rates with the acid amount of Zn_x/S-1 (determined by the NH_3-TPD method), we obtained a linear dependence of isobutane conversion on the total acid amount of Zn_x/S-1 (Fig. 10). This meant that the acid sites of Zn_x/S-1 played a critical role in isobutane conversion. The yield of undesired dry gases was significantly suppressed, perhaps due to the absence of strong acid sites. Furthermore, the true role of different categories of acid sites of Zn_x/S-1 in isobutane conversion still needs to be identified, with investigations currently underway in our laboratory.

4 Conclusions

In summary, the inert S-1 zeolite was significantly acidified by modification with Zn. Both Lewis acid sites and a small amount of Brønsted acid sites were identified in Zn_x/S-1 catalysts. Using UV-Vis and FT-IR analysis, we found that the Lewis and Brønsted acid sites of Zn_x/S-1 were associated with small ZnO clusters and external Zn–OH groups on ZnO clusters, respectively. Furthermore, the linear relationship between isobutane conversion and total acid amount suggested that the acid sites of Zn_x/S-1 played a crucial role in isobutene conversion. Zn_x/S-1 catalysts exhibited excellent isobutane dehydrogenation and butene isomerization activities, and the yield of undesired dry gas (methane and ethane) was significantly suppressed because strong acid sites were absent. A high selectivity of total butene products ranging from 84.6 to 97.2 was achieved on the catalysts with different Zn loading. Therefore, Zn-modified S-1 zeolites can be applied to the highly efficient transformation of light alkanes.

Conflicts of interest

The authors have no conflicts of interest to declare.

Acknowledgements

This work was supported by National Natural Science Foundation of China (No. 21603023).

Notes and references

1 V. Bolis, C. Busco, S. Bordiga, P. Ugliengo, C. Lamberti and A. Zecchina, *Appl. Surf. Sci.*, 2002, **196**, 56–70.
2 G. P. Heitmann, G. Dahlhoff and W. F. Hölderich, *J. Catal.*, 1999, **186**, 12–19.
3 H. Ichihashi and H. Sato, *Appl. Catal., A*, 2001, **221**, 359–366.
4 H. Ichihashi, M. Ishida, A. Shiga, M. Kitamura, T. Suzuki, K. Suenobu and K. Sugita, *Catal. Surv. Asia*, 2003, **7**(4), 261–270.
5 B. Bonelli, L. Forni, A. Aloise, J. B. Nagy, G. Fornasari, E. Garrone, A. Gedeon, G. Giordano and F. Trifirò, *Microporous Mesoporous Mater.*, 2007, **101**, 153–160.
6 E. Janiszewska, A. Macario, J. Wilk, A. Aloise, S. Kowalak, J. B. Nagy and G. Giordano, *Microporous Mesoporous Mater.*, 2013, **182**, 220–228.
7 M. Bernaue, E. Tabor, V. Pashkova, D. Kaucký, Z. Sobalík, B. Wichterlová and J. Dedecek, *J. Catal.*, 2016, **344**, 157–172.
8 L. B. Young, S. A. Butter and W. W. Kaeding, *J. Catal.*, 1982, **76**(2), 418–432.
9 S. Ilias and A. Bhan, *J. Catal.*, 2014, **311**, 6–16.
10 Y. Ni, A. Sun, X. Wu, G. Hai, J. Hu, T. Li and G. Li, *Microporous Mesoporous Mater.*, 2011, **143**(2), 435–442.
11 M. Guisnet, N. S. Gnep, D. Aittaleb and Y. J. Doyemetet, *Appl. Catal., A*, 1992, **87**(2), 255–270.
12 J. J. H. B. Sattler, J. Ruiz-Martinez, E. Santillan-Jimenez and B. M. Weckhuysen, *Chem. Rev.*, 2014, **114**(20), 10613–10653.
13 T. Otroshchenko, J. Radnik, M. Schneider, U. Rodermerck, D. Linke and E. V. Kondratenko, *Chem. Commun.*, 2016, **52**, 8164–8167.
14 J. A. Biscardi, G. D. Meitzner and E. Iglesia, *J. Catal.*, 1998, **179**, 192–202.
15 Y. G. Kolyagin, V. V. Ordomsky, Y. Z. Khimyak, A. I. Rebrovc, F. Fajulad and I. I. Ivanova, *J. Catal.*, 2006, **238**, 122–133.
16 Y. G. Kolyagin, I. I. Ivanova and Y. A. Pirogov, *Solid State Nucl. Magn. Reson.*, 2009, **35**, 104–112.
17 G. Caeiro, R. H. Carvalho, X. Wang, M. A. N. D. A. Lemosa, F. Lemosa, M. Guisnet and F. R. Ribeiro, *J. Mol. Catal. A: Chem.*, 2006, **255**, 131–158.
18 Y. J. Ren, F. Zhang, W. M Hua, Y. H Yue and Z. Gao, *Catal. Today*, 2009, **148**, 316–322.
19 A. W. Aldag and B. Okla, *US pat.* 4,524,144, 1985.
20 Z. X. Chen, A. Derking, W. Koot and M. P. van Dijk, *J. Catal.*, 1996, **161**, 730–741.
21 N. M. Schweitzer, B. Hu, U. Das, H. Kim, L. A. Curtiss, P. C. Stair, T. Miller and A. S. Hock, *ACS Catal.*, 2014, **4**, 1091–1098.
22 L. Q. Wang, X. S. Wang and X. W. Guo, *Chin. J. Catal.*, 2001, **22**, 513–514.
23 J. Chen, Z. Feng, P. Ying and C. Li, *J. Phys. Chem. B*, 2004, **108**, 12669–12676.
24 Y. M. Ni, W. Y. Peng, A. M. Sun, W. L. Mo, J. L. Hu, T. Li and G. X. Li, *J. Ind. Eng. Chem.*, 2010, **16**, 503–505.
25 H. A. Zaidi and K. K. Pant, *Catal. Today*, 2004, **96**, 155–160.
26 F. Yin, A. L. Blumenfeld, V. Gruver and J. J. Fripiat, *J. Phys. Chem. B*, 1997, **101**, 1824–1830.
27 W. Zhang, P. G. Smirniotis, M. Gangoda and R. N. Bose, *J. Phys. Chem. B*, 2000, **104**, 4122–4129.
28 V. S. Escribanoa, T. Montanarib and G. Busca, *Appl. Catal., B*, 2005, **58**, 19–23.
29 G. V. A. Martins, G. Berlie, C. Bisio, S. Coluccia, H. O. Pastore and L. Marchese, *J. Phys. Chem. C*, 2008, **112**, 7193–7200.
30 E.-M. El-Malki, R. A. van Santen and W. M. H. Sachtler, *J. Phys. Chem. B*, 1999, **103**, 4611–4622.
31 S. S. Arzumanov, A. A. Gabrienko, D. Freude and A. G. Stepanov, *Solid State Nucl. Magn. Reson.*, 2009, **35**, 113–119.
32 K. J. Caspary, H. Gehrke, M. Heinritz-Adrian and M. Schwefer, *Handbook of Heterogeneous Catalysis*, Wiley, 2nd edn, 2008, pp. 3206–3229.